March 2012

Interlayer coupling effects in $SrTiO_3$ bilayer delta-doped structures

Department of Advanced Material Science, 47106003, Hisashi Inoue,

Adviser: Professor Hiroshi Okamoto

Keywords: perovskite oxides, delta-doping, coupling, subband quantization, two-dimensional, multi-band superconductivity

[Introduction]

Layered superconductors such as cuprates, organics and pnictides are intensely studied in the bulk. In these systems, the two-dimensional (2D) character and the coupling between the adjacent superconducting layers is a key ingredient for their novel properties [1-3]. These fascinating materials can be naturally imitated by artificial thin film heterostructures, where greater degrees of freedom and control exist. However, up to now these superlattices have been limited by their relative small mean free paths l. Layered artificial 2D superconductors in the clean limit have not been explored, although novel superconducting phases such as the Fulde-Ferrel-Larkin-Ovchinnikov (FFLO) state [4,5] are suggested theoretically.

Recently, steps towards this limit were made by confining the superconducting electrons in a $SrTiO_3$ heterostructure in a narrow delta-doped region. Thanks to its low critical carrier density and high mobility, l is enhanced to such a degree that a 2D quantization becomes important. Recent study revealed that subbands were created in the $SrTiO_3$ (STO) delta-doped structure and also showed 2D superconductivity [6]. The investigation of this confinement effect is interesting since discrete superconducting states should exist in each subband, if the subband splitting energy is much larger than the superconducting condensation energy.

However in a single delta-doped layer there was no clear evidence for such discrete superconducting states. We investigate the link between subband creation and superconductivity by making bilayer delta-doped structure [Fig. 1] with variable coupling strength. This modulation changes the subband structure, from which we can detect the subband effects on superconductivity.

[Experimental details]

High quality STO bilayer delta-doped structures with different undoped interlayer thickness d_{inter} were fabricated by pulsed laser deposition depositing STO and 0.5 wt.% Nb:STO single crystal targets sequentially (Fig. 1)[7]. The doped layer thickness, d_{doped}, was fixed at 6 nm, and the subband structure was tuned by varying d_{inter} in the range 3.7 nm to 270 nm. The normal state and superconducting properties were characterized by magneto-transport measurements in a pumped helium cryostat or dilution refrigerator.

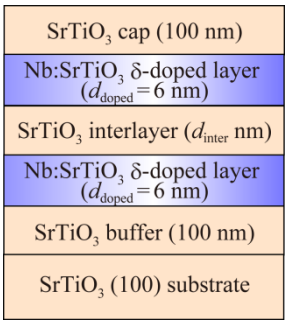

Fig. 1. Schematic diagram of the STO bilayer delta-doped structure.

[Results & Discussion]

1. Normal state properties

First we examined the effect of coupling on the normal state properties at T = 2 K. Fig. 2(a) shows the dependence of the of sheet resistance (ρ_{xx}) on the interlayer thickness. A clear decrease in ρ_{xx} was observed for intermediate d_{inter}. For large d_{inter}, ρ_{xx} was about the half of that for single delta-doped samples, indicating that the two doped layers were decoupled in this range.

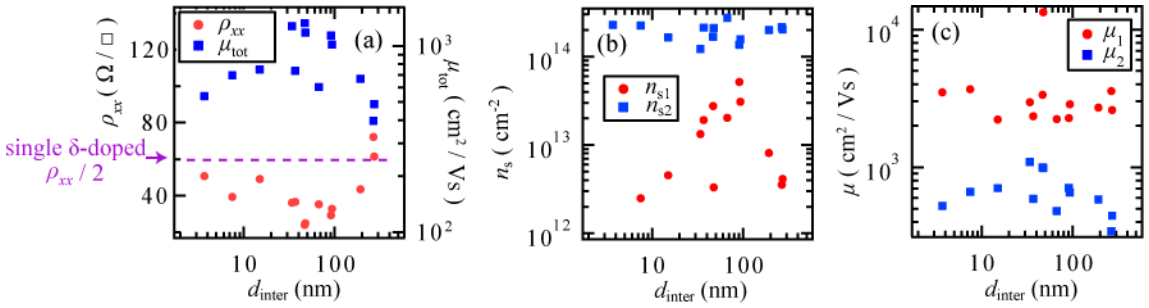

Fig. 2. d_{inter} dependence of (a) sheet resistance and total mobility, (b) two sheet carrier densities and (d) carrier mobility for each component measured at T = 2 K.

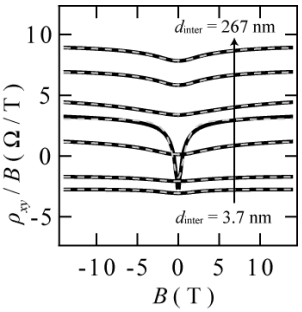

Fig. 3. Fitting results for Hall coefficient ρ_{xy}/B, where B is the magnetic flux density. The solid and broken lines indicate experimental data and fitting curves respectively.

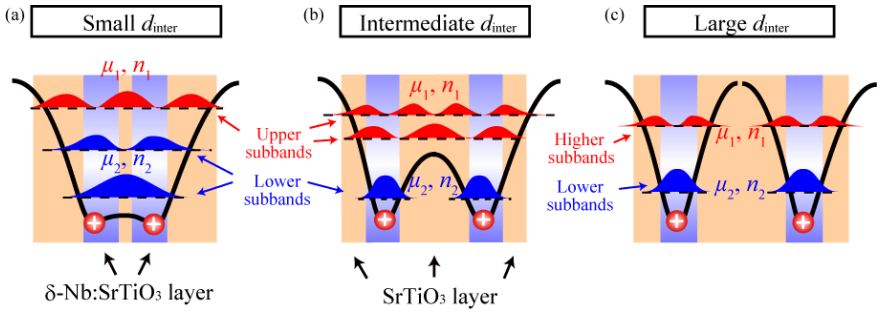

Fig. 4. Schematic diagram of the subband structure in STO bilayer delta-doped systems for (a) small, (b) intermediate and (c) large d_{inter}.

In order to examine the origin of resistance drop, Hall measurements were performed. The Hall resistance ρ_{xy} clearly showed nonlinearity, which can be attributed to existence of multiple conduction channels with different mobility and carrier density [8]. Assuming there were two groups of carriers, the sheet carrier densities n_{s1}, n_{s2} and mobilities μ_1, μ_2 were extracted by fitting, which showed good agreement with the results (Fig.3.) The dependence of the total mobility $\mu_{tot} = (\mu_1 n_{s1} + \mu_1 n_{s1})/(n_{s1} + n_{s2})$ is shown in Fig. 2(a). The enhancement of μ_{tot} at intermediate d_{inter} range was clearly the origin of the resistance drop. Based on the assumption of a 3D Fermi sphere, l was calculated, using the relation $l = m^* v_F / n_s e^2 \rho_{xx}$ where m^* is the electron effective mass, v_F is the Fermi velocity, e is the elemental charge. We confirmed that l was significantly larger than the d_{doped}, indicating that the system was in quasi-2D limit for all d_{inter}.

The mechanism under the enhancement of μ_{tot} was related to carrier transfer from low mobility state to high mobility state. The number of high mobility carriers n_{s1} showed similar trends to μ_{tot} while μ_1 and μ_2 remained almost constant [Fig.2(c) & (d)]. This can be interpreted from the subband structure in Fig. 4. In the large d_{inter} regime, upper and lower subbands were confined in each doped layer, separated by a large potential barrier at the interlayer [Fig. 4(a)]. So the electrons in the upper subbands and lower subbands had similar value of μ since they had the same probability of scattering by the dopant at the doped layer. Only a few electrons at the top of the subband had higher μ with less probability of scattering thanks to the larger penetration into the undoped layer. When d_{inter} decreased from this decoupled range, due to the layer coupling, the confinement potential at the interlayer is expected to decrease at the same time [Fig. 4(b)]. In this regime more electrons in the upper subband can spread into the interlayer, and exhibit higher mobility. As d_{inter} is further decreased, however, the electrons in the upper subbands again experience relatively large scattering at the dopant layers due to the narrow confinement [Fig. 4(c)]. The slight increase of μ_2 for intermediate d_{inter} might come from the larger penetration into undoped interlayer due to the lower potential barrier.

2. Superconductivity

The superconducting properties were investigated by measuring the superconducting upper critical field H_{c2}. As expected for a 2D superconductor, all samples showed a strong H_{c2} anisotropy with field inclination angle (θ) measured with respect to the film surface, reflecting the suppression of orbital depairing in the in-plane geometry. For samples with thinner and thicker d_{inter} (an example is shown in the inset of Fig. 5), the $H_{c2}(\theta)$ data could be well fitted to the standard form for a 2D superconductor [9]:

$$|H_{c2}(\theta)\sin\theta/H_{c2}^{\perp}| + \left(H_{c2}(\theta)\cos\theta/H_{c2}^{\parallel}\right)^2 = 1 \qquad (1)$$

where $H_{c2}^{\perp}$ is the perpendicular ($\theta = 90°$) critical field and $H_{c2}^{\parallel}$ is the parallel ($\theta = 0°$) critical field. However for intermediate d_{inter}, (Fig. 5),

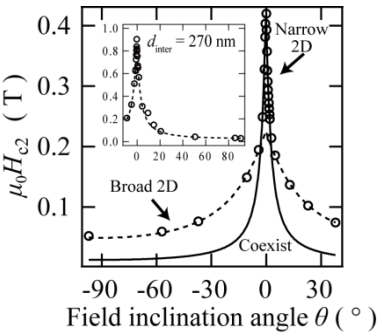

Fig. 5. Angular dependence for an intermediate d_{inter}. Open circles correspond to experimental data and dashed and solid lines indicate the fitting results using Eq. (1) for the two respective components. Inset: The θ-dependence for a large d_{inter}.

this simple fit was not possible, indicating the existence of multiple superconducting components. In this case we fitted the data by Eq. (1) using two sets of parameters $H_{c2}^{\perp}$ and $H_{c2}^{\parallel}$ at high and low θ.

We estimated the spatial distribution of the superconductivity, d_{SC}, in the growth direction from the equation: $d_{SC} = (6\Phi_0 H_{c2}^{\perp}/\pi H_{c2}^{\parallel 2})^{1/2}$ where Φ_0 is the flux quantum and the other parameters were obtained from the theoretical fits to Eq. (1). The results are shown in Fig. 6. For small d_{inter} region, d_{SC} followed the total thickness of layers $d_{tot} \sim d_{inter} + 2d_{doped}$, suggesting that the superconductivity spreads into the undoped spacer layer. In the intermediate d_{inter} regime, we obtained multiple d_{SC} components: one had $d_{SC} \sim d_{doped}$, which corresponds to the relatively higher value of H_{c2} around $\theta = 0°$ forming narrow 2D state around the doped layer. Another component near $\theta = 90°$ had a thickness closer to d_{tot}, representing the superconductivity spreading into the spacer layer. When d_{inter} was as large as $d_{inter} = 267$ nm, again only one component of thickness $\sim d_{doped}$ is observed, indicating superconductivity is localized around each delta-doped layer. These data can be understood from the subband picture discussed above. In the small d_{inter} range, the upper subbands dominate the superconductivity since d_{tot} corresponds to the spatial distribution of upper subbands [Fig. 4(a)]. In the intermediate d_{inter} region, subbands with different spatial distribution coexist as shown in Fig. 4(b) due to slightly larger potential barrier in the interlayer. The lower subbands were localized in each delta-doped layer, which condensed into superconducting state forming the component of $d_{SC} \sim d_{doped}$ while the upper subbands spread over the two delta-doped layers which showed superconductivity with $d_{SC} \sim d_{tot}$. In this case, the angular dependence was expressed as a superposition of the upper and lower subbands, consistent with the dependence in Fig. 5. We note that in low field range near $\theta = 0°$, both narrow and broad 2D superconducting states coexist. When d_{inter} become large enough to decouple the layers, d_{SC} decreased to d_{doped} since these subbands were confined to each layer separated by the large potential barrier in the interlayer [Fig. 4(b)].

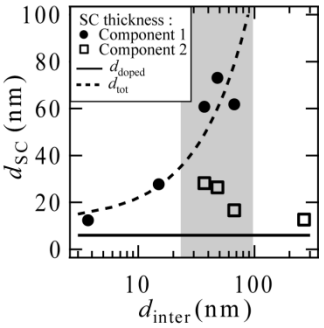

Fig. 6. Variation of d_{SC} with d_{inter}. The filled area indicates the regime where we obtained multiple components from the experiments.

[Conclusion]

We demonstrated the effect of coupling on the normal states and superconducting state properties in STO bilayer delta-doped structures. The existence of multiple types of carriers in normal state and variation of superconducting order parameter by interlayer thickness as well as the abnormal angular dependence of upper critical field were observed. These results were understood from the subband creation due to 2D confinement. This model also suggests the coexistence of different superconducting states with different spatial distribution. These results provide significant information for the investigation of controlled superconducting systems in a subband quantized regime, which may impact recent studies of high T_c superconductors [10] as well as other layered superconductors.

[References]

[1] A. A. Tsvetkov *et al.*, *Nature*. **395**, 360 (1998).
[2] Y-M. Xu *et al.*, *Nat. Phys.* **7**, 198 (2011).
[3] T. Shibauchi *et al.*, *Phys. Rev. B* **55**, R11977 (1997).
[4] P. Fulde *et al.*, *Phys. Rev.* **135**, A550 (1964).
[5] A. I. Larkin *et al.*, *Sov. Phys. JETP* **20**, 762 (1965).
[6] Y. Kozuka *et al.*, *Nature* **462**, 487 (2009).
[7] Y. Kozuka *et al.*, *Appl. Phys. Lett.* **97**, 222115 (2010).
[8] M. J. Kane *et al.*, *J. Phys. C : Solid State Phys.* **18**, 5629 (1985).
[9] M. Tinkham, *Phys. Rev.* **129**, 2413 (1963).
[10] D. Nicolas *et al.*, *Nature* **447**, 565 (2007).

[Presentations and Publications]

A) H. Inoue, M. Kim, C. Bell, Y. Hikita, H. Y. Hwang, JPS 66th Spring Meeting, Niigata, Japan (2011).

* One more presentation as the first author to be presented at the APS March Meeting, Boston, USA (2012).